Title

Axial variation of deoxyhemoglobin density as a source of BOLD low-frequency time lag structure

Authors

Toshihiko Aso[1,2*], Shinnichi Urayama[2,3], Fukuyama Hidenao[2,3], Toshiya Murai[1]

Affiliations

[1]Department of Psychiatry, Kyoto University Graduate School of Medicine, Kyoto, Japan

[2]Human Brain Research Center, Kyoto University Graduate School of Medicine, Kyoto, Japan

[3]Research and Educational Unit of Leaders for Integrated Medical System, Center for the Promotion of Interdisciplinary Education and Research, Kyoto University, Kyoto, Japan

*** Correspondence:**

Toshihiko Aso
aso.toshihiko@gmail.com

Keywords

BOLD contrast, Low-frequency oscillations, Cerebral blood flow, Neurovascular coupling, Resting-state fMRI, Image denoising

Abstract

Perfusion-related information is reportedly embedded in the low-frequency component of blood oxygen level-dependent (BOLD) fMRI signal. The blood-propagation pattern through the cerebral vascular tree is detected as an interregional lag variation of spontaneous low-frequency oscillations (sLFOs). Mapping of this lag, or phase, has been implicitly treated as a projection of the vascular tree structure onto real space. While accumulating evidence supports the biological significance of this signal component, the physiological basis of the "perfusion lag structure," a requirement for an integrative fMRI-signal model, is lacking. In this study, we conducted analyses furthering the hypothesis that the sLFO is not only largely of systemic origin, but also essentially intrinsic to blood and hence, behaves as a virtual tracer. By summing the small fluctuations of instantaneous phase differences between adjacent vascular regions, a velocity response to respiratory challenges was detected. Regarding the relationship to neurovascular coupling, the removal of the whole lag structure, which can be considered as an optimized global-signal regression, resulted in a reduction of signal variance, while preserving the fMRI response. Examination of the T2* and S_0, or non-BOLD,

components of the fMRI signal revealed that the lag structure is deoxyhemoglobin-dependent, while paradoxically presenting a signal-magnitude reduction in the venous side of the cerebral vasculature. These findings provide insight into the origin of BOLD sLFO, at least partly intrinsic to the circulating blood.

1 Introduction

In efforts to improve the efficiency of functional magnetic resonance (MR) imaging (fMRI), studies have revealed various systemic physiological components in blood oxygen level-dependent (BOLD) signal fluctuations. Physiological parameters, such as cardiac pulsation (Chang et al., 2009), respiration (Birn et al., 2006), blood pressure, and end-tidal CO_2 (Murphy et al., 2013; Wise et al., 2004), are considered artifact sources. These phenomena are supposed to bypass neurovascular coupling (NVC) and, therefore, to cause neuro-BOLD *un*coupling that can confound fMRI analysis. The contamination by such components is expected to be emphasized in resting-state fMRI (rs-fMRI), where signals are evaluated without trial averaging (Winder et al., 2017). However, discrimination between neuronal and non-neuronal components has never been a simple matter due to the lack of validation techniques with comparable spatial and temporal precisions to those of fMRI.

In the last decade, the relationship between the low-frequency oscillation (LFO, < 0.1 Hz) of systemic circulation and the BOLD signal has garnered increasing attention (Tong et al., 2017; Zhu et al., 2015). One major spontaneous LFO (sLFO) affecting fMRI would be the respiratory volume fluctuation involving a chemoreflex loop (Birn et al., 2008). Classically, an sLFO in blood pressure, known as the Traube–Hering–Mayer wave, has been shown to originate from another autonomic loop (Guyton and Harris, 1951; Julien, 2006). Associated sLFOs in blood flow and velocity have also been found (Fagrell et al., 1977; Killip, 1962), and, later, transcranial Doppler ultrasonography and optical methods confirmed their traces within the brain (Giller et al., 1999; Obrig et al., 2000). This sLFO in the optical signals was found in both oxy- and deoxy-hemoglobin (Hb) with an interesting, but still unresolved, phase difference exclusively observed in the brain (Rayshubskiy et al., 2014; Tgavalekos et al., 2016). Furthermore, sLFO was found even in electroencephalographic recordings, for which cerebral vasomotion was suggested as the origin (Nikulin et al., 2014), although it is unclear to what extent the arterial vasomotion accounts for the fMRI signal.

As mentioned above, Hb-sLFO was postulated to be of systemic origin (Katura et al., 2006; Sassaroli et al., 2012; Tian et al., 2011). Hence it was not entirely surprising to find a correlation between the global fMRI signal and extra-cerebral NIRS or MRI signals, but the constant time shift, or phase difference, across body or brain parts was unexpected (Anderson et al., 2011; Tong et al., 2012). The demonstration of the similarity between the low-frequency lag map and perfusion MRI in healthy participants was a milestone in this direction, by clearly presenting the perfusion time lag embedded in the BOLD signal (Tong et al., 2017). The resilient nature of the lag map against an fMRI

task condition was shown in our previous study, further supporting its non-neuronal origin (Aso et al., 2017a). In parallel, clinical studies started to establish the phase delays as a marker of cerebrovascular disorders (Amemiya et al., 2013; Christen et al., 2015; Khalil et al., 2018; Lv et al., 2013; Ni et al., 2017; Nishida et al., 2018). Gross vascular anatomy has been detected consistently in these studies, replicating the results from respiratory challenges (Blockley et al., 2011; Chang and Glover, 2009b), which, importantly, suggests an equivalence between the sLFO and manipulated circulatory turbulences. Apart from patient data, a recent study involving healthy participants revealed changes in venous drainage pattern with normal aging (Satow et al., 2017). A body of evidence thus empirically supports the biological significance of the low-frequency lag structure and its underlying principles.

The current analytical model of the BOLD lag structure assumes the presence of this signal variation from the very early stages of cerebral perfusion (Tong et al., 2018)(**Fig. 1A**). Such synchronized variation should naturally affect the global mean signal and the model is hence related to the unresolved fMRI global signal problem (Liu et al., 2017; Power et al., 2017). This view is not only compatible with the occasional favorable effect of global signal regression (GSR) in task fMRI (Aguirre et al., 1998) but has led some scientists to propose the removal of the whole lag structure as an approach for noise elimination (Amemiya et al., 2016; Byrge and Kennedy, 2018; Erdoğan et al., 2016). Under this model, the elimination of the lag structure can be viewed as an optimized GSR (of the low-frequency component) for each voxel group. Conversely, with the presence of the BOLD lag structure, a simple GSR should retain a residual correlation between in-phase voxels that confounds fMRI analyses (Erdoğan et al., 2016; Taylor Webb et al., 2013).

The fundamental and critical question remaining to be addressed is the mechanism by which sLFO (or respiratory maneuvers) creates the BOLD lag structure. The BOLD response to neural activity via NVC is a well-documented passive process, involving the expansion of the intravascular compartment (Herman et al., 2009). A typical model of the BOLD signal change is described as follows (Hoge et al., 1999):

$$\frac{\Delta BOLD}{BOLD_0} = M\left(1 - \left(\frac{CMRO_2}{CMRO_2|_0}\right)^{\beta}\left(\frac{CBV}{CBV_0}\right)\left(\frac{CBF}{CBF_0}\right)^{-\beta}\right) \qquad [1],$$

where $CMRO_2$ stands for the cerebral metabolic rate of oxygen in a voxel, CBV/CBF for cerebral blood volume and flow, respectively. Beta is an exponent of the power-law describing the relationship between T2* and deoxygenated Hb (deoxy-Hb) amount that only depends on $CMRO_2$ and CBF in a reciprocal manner, under the assumption of negligible inflow of deoxy-Hb. M is the factor for the BOLD susceptibility effect defined as:

$$M \equiv TE \cdot B_0 \cdot CBV_0 \cdot [dHb]_{V0}^{\beta} \qquad [2],$$

where B_0 is the main magnetic field strength. Triggered by vasodilation of the arteriole, this effect is diminished by an inflow of fresh blood, which increases the MR signal primarily in the venous side

of the activated site (Buxton, 2012). In another line of studies, this baseline BOLD effect has been modelled in the formula for the off-resonance frequency shift as follows (An and Lin, 2002; Yablonskiy and Haacke, 1994):

$$\boldsymbol{\delta\omega = \gamma \cdot \frac{4}{3} \cdot \pi \cdot \Delta\chi_0 \cdot Hct \cdot OEF \cdot B_0} \qquad [3],$$

where γ is the gyromagnetic ratio (42.58 MHz/T), $\Delta\chi_0$ is the susceptibility difference between the fully oxygenated and fully deoxygenated blood, and Hct is the hematocrit (volume fraction of erythrocytes to the blood volume, typically around 40%). The oxygen extraction fraction (OEF), sometimes referred to as oxygen extraction ratio (OER), represents the only source of deoxy-Hb, again, under the assumption of 100% oxygen saturation (SaO_2) in the inflow. Variation of this base susceptibility can occur due to the local Hct and SaO_2 changes and, in fact, has been shown to cause intersession variabilities (Cohen et al., 2002; Tuunanen and Kauppinen, 2006), but within-session fluctuations have rarely been considered (Thomas et al., 2000). For example, even at a constant Hb density and oxygen partial pressure, CO_2 fluctuation, a driving factor of vasomotion, alone can modify SaO_2 through pH changes (Collins et al., 2015a). Although the assumption of constant base deoxy-Hb concentration may be sufficient for modeling its dilution by NVC (Ogawa et al., 1998), other effects might not be negligible in non-neuronal fluctuations (Winder et al., 2017)(**Fig. 1b**).

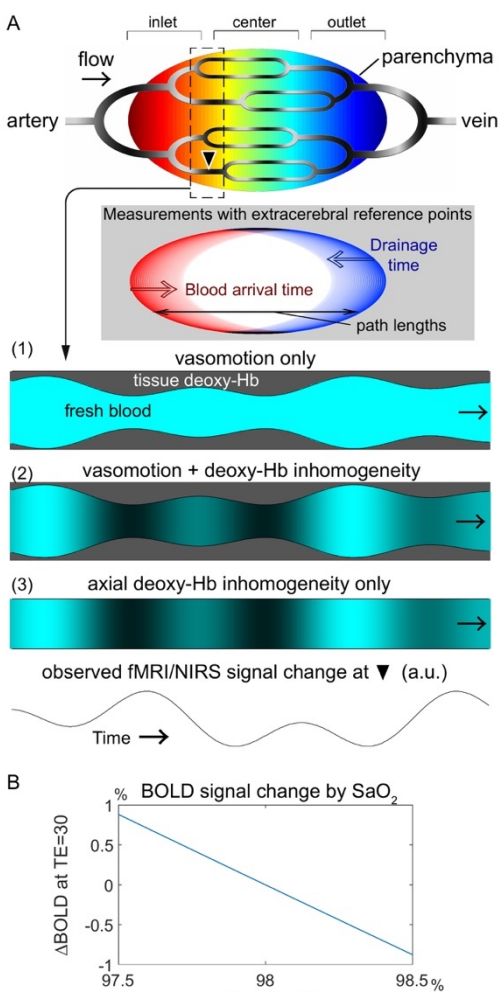

Fig. 1. Working model of the BOLD lag mapping. *A*, Schematic of the cerebral vascular tree presenting possible physiological models that account for the fMRI and NIRS observations. Each brain voxel has its lag (phase) of the spontaneous low frequency oscillation (sLFO) relative to the reference point, depicted in warm and cool colors. Another schematic is inserted to illustrate the effect of the reference point selection in relation to the vascular path length, which accounts for the disagreement with other blood-tracking techniques. Below are shown three models with different physiological signal sources that are moving along the vasculature. While vasomotion can be a major source of this sLFO (1), axial inhomogeneity of the deoxy-hemoglobin (Hb) density may also contribute even in the absence of vasomotion and flowmotion (2,3). The moving axial inhomogeneity creates a similar temporal profile with varying lag across regions. *B*, Dependence of the BOLD signal on inflow oxygen saturation (SaO2), a major determinant of deoxy-Hb concentration, at 3 T, TE = 30 ms. All other parameters were maintained constant at physiological values: oxygen extraction fraction = 45%, tissue blood volume fraction = 3%, and hematocrit = 40% (see Eqs. [1] and [2]).

In this exploratory study, we conducted three investigations to further advance our knowledge on the BOLD lag structure and its underlying physiology. We first evaluated if changes in blood transit velocity are embedded in the BOLD low-frequency phase to confirm its behavior as a virtual tracer [a preliminary analysis of these data was presented previously as a poster (Aso et al., 2017b)]. Next, we investigated the effect of eliminating the lag structure from task-based fMRI, which has not been tested yet. Finally, we used multi-echo imaging to assess the components of the BOLD signal that determine the lag structure. One of the recent approaches toward fMRI denoising has focused on S_0 fluctuation (signal at echo time = 0, which is the baseline MR signal from the fluid compartments), as it is weakly associated with neural activity (Kundu et al., 2012; Posse et al., 1999; Wu et al., 2012; Yen et al., 2017). In contrast, the total-Hb sLFO, detected by NIRS, is interpreted as a local CBV change under the assumption of a constant Hct, which should also affect the non-BOLD component via changes in plasma volume and inflow (Rostrup et al., 2005). Again, the T2* and S_0 components may contribute in a different manner than NVC to the BOLD lag structure that have been overlooked in studies based on trial averaging. From the influences of three different fMRI task paradigms, including a simple reaction-time visuomotor task, a short breath-holding task, and a hyperventilation task on the neural and non-neural components of the fMRI signal, we sought further validation of our hypothetical model of the BOLD lag structure.

2 Materials and methods

2.1 Subjects and experimental procedures

Twenty-one healthy subjects (eight women, 19–26 years of age) participated in Experiment 1; one subject was excluded from the analysis because of abrupt head motion, which prevented BOLD lag mapping (see Data processing). The remaining 20 participants performed the sparse visuomotor and 10-s breath-holding tasks, but the hyperventilation task was only performed by 18 participants, as it was introduced after the first two participants had concluded their participation in the study. Another 21 participants were recruited for Experiment 2, involving multi-echo acquisition, all of whom performed the above three tasks but with an 18-s version of the breath-holding task. To avoid vigilance level fluctuations, all MRI sessions were scheduled in the morning and the participants were encouraged to sleep well the previous night.

The protocol for this study was approved by the internal ethics review board of Kyoto university. The subjects provided written informed consent in advance, according to the Declaration of Helsinki, for the analysis of anonymized MRI scans and simultaneously acquired physiological data.

2.2 Image acquisition

A Tim-Trio 3-Tesla scanner (Siemens, Erlangen, Germany) with a 32-channel phased-array head coil was used for MRI acquisition. For Experiment 1, T2*-weighted echo-planar images were acquired using multiband gradient-echo echo-planar imaging (EPI) (Feinberg et al., 2010) with the following

parameters to cover the entire cerebrum: 64 × 64 pixels, interleaved 35 slices, 192-mm field of view (FOV), 3.5-mm slice thickness, repetition time (TR)/echo time (TE) = 500/35 ms, flip angle = 40°, and multiband factor of five. Three 9-min runs (1,080 volumes) were acquired for each of the three task conditions. The same pulse sequence program was used in Experiment 2 but with multi-echo settings: TE1 = 7.76 ms and TE2 = 25.82 ms for the first six subjects and TE1 = 11.2 ms and TE2 = 32.78 ms for the remaining 15 subjects. A smaller multiband factor of two was selected to allow for the short TE in combination with a parallel imaging using GRAPPA. Other acquisition parameters were: TR = 1,300 ms, flip angle = 65°; interleaved 36 slices, FOV = 256 × 192 mm^2, 64 × 48 matrix, 3.5-mm slice thickness. Three 7-min (323 TRs) runs were acquired. Seven subjects in Experiment 2 underwent two additional runs with a shorter TR of 700 ms and a flip angle of 45° to examine the sensitivity of the respiration-related signal component to inflow modulation. At the end of every experimental session, a 3D MPRAGE T1-weighted image was acquired for obtaining anatomical information (Aso et al., 2017a). A dual-echo gradient-echo dataset for B0 field mapping was also acquired after the BOLD scan in the same orientation.

2.3 Task conditions

Throughout the experimental session, task instructions were presented via an LCD monitor inside the scanner room, viewed through a mirror. Beat-to-beat fluctuations in the mean arterial pressure and heart rate were obtained via a non-invasive MR-compatible device (Caretaker, BIOPAC Systems, Inc., Goleta, CA, USA). Careful instructions were provided to the participants on how to avoid motion, especially during the respiratory challenges.

2.3.1 Sparse visuomotor task

A simple visuomotor task with a varying intertrial interval of 6 to 24 s was performed during the first run. Subjects were instructed to press a button with their right index finger as soon as the computer screen changed from “Please hold still” to “Press the button.” The screen returned to “Please hold still” at the button press or after 3 s, if the participant had not pressed the button.

2.3.2 Breath-holding task

To minimize head motion induced by the tasks, the two respiratory challenges were adapted to be less strenuous than in earlier studies. In Experiment 1, the breath-holding task was cued by a “Hold your breath” instruction on the screen, at which point the subjects were asked to immediately hold their breath, irrespective of the respiration phase. The holding periods lasted for 10 s and were separated by 90-s intervals. This short duration was selected to minimize strain that can cause body movements, while evoking a detectable autoregulatory response (Murphy et al., 2011). In Experiment 2, a longer holding period of 18 s after a brief inhalation for 2 s was used to evoke a more pronounced vasodilation.

2.3.3 Hyperventilation task

The hyperventilation task involved paced breathing at 1/5 Hz for 25 s, separated by a 30-s rest. Each 5-s cycle began with the screen presenting “Please inhale” for 1.5 s, followed by “Please exhale slowly,” lasting 3.5 s. Subjects were instructed to breathe as deeply as possible, while avoiding head movement. A short inspiration period was selected to suppress motion by minimizing movements in the thoracic cage and spine.

2.4 Data processing

For image processing, SPM12 (Wellcome Department of Cognitive Neurology, London, United Kingdom) and FSL5 (FMRIB Software Library, www.fmrib.ox.ac.uk/fsl) (Smith et al., 2004) were used in combination with in-house MATLAB scripts. Off-resonance geometric distortions in the EPI data were corrected using FUGUE/FSL with B0 field maps. After inter-scan slice-timing correction, head motion was compensated by 3D motion correction and data repair (Mazaika et al., 2009). The repairing procedure aimed to remove motion-related signal dropout and involved searching for time points satisfying two stringent criteria: (1) global signal change between consecutive volumes exceeding 1% and (2) head displacement exceeding a Euclidian distance of ±1 mm or ±1° rotation per TR. The affected time points were replaced with linearly interpolated values, but this procedure was required in only six of the 41 participants. The data were further cleaned by regressing out 24 head motion-related parameters. Unlike in previous studies, the six rigid-body parameter timeseries were not directly used because of the possible contamination of the motion parameters with the global signal when the subjects were immobile (Freire and Mangin, 2001). We used the first temporal derivatives of the motion parameters, their shifted versions by 1 TR, and the squares of those 12 timeseries (Satterthwaite et al., 2013). Images were spatially normalized to the template space using the T1-weighted anatomical image and resliced to a 4-mm isotropic voxel size to achieve a high voxel temporal signal-to-noise ratio.

2.4.1 Lag mapping

A recursive technique was used (Aso et al., 2017a) after temporal bandpass filtering at 0.008–0.07 Hz to ensure that the phase was uniquely determined within the cross-correlation range. Whereas lag was tracked up to 7 s in both directions, upstream and downstream, for most analyses, it was limited to 4 s for the calculation of the relative BOLD transit time (rBTT, see below). This shorter tracking range allowed a higher cutoff frequency (0.12 Hz) to preserve the high-frequency component in the velocity change profiles.

The global mean signal was used to select the initial seed that defined the reference phase (lag = 0). First, voxels presenting a cross-correlogram peak at 0 with the global signal were determined. The time course averaged over this set of voxels served as the initial reference. In each step of the recursive procedure towards up- and downstream, a cross-correlogram was calculated between the timeseries obtained from the previous seed voxels and every undetermined voxel to find a set of

voxels with a peak at ± 0.5 s, which then served as the new seed. This tracking part retained some voxels without any lag values because cross-correlogram peaks < 0.3 were not used (Tong et al., 2017). These voxels were later filled one by one with average phases from voxels with similar time courses at correlation coefficients > 0.3. There were single isolated holes even after this procedure, which were filled by linear interpolation, using the six neighbors.

2.4.2 fMRI analysis on "cleaned" BOLD datasets

Individual BOLD data from Experiment 1, after the above pre-processing steps including the motion parameter regression, served as the reference or "raw" dataset. GSR with low-pass filtered global signal, normal GSR, global scaling implemented in SPM12, and removal of the perfusion lag structure ("deperfusioning") were compared with the raw dataset.

The GSR involves regression by the global signal and extracting the residuals in each voxel. In deperfusioning, instead of the uniform regressor, a corresponding timeseries was used for each voxel group by the lag value ("dynamic" GSR) (Erdoğan et al., 2016). For global scaling, the raw dataset was entered into the same SPM pipeline, except for the option of internally dividing each volume by its global mean signal instead of the constant session mean. The normal GSR and global scaling thus affected all frequency ranges, whereas the filtered GSR and deperfusioning removed only the low-frequency components.

Random effects analysis (Friston et al., 2002) was used to evaluate the effect of these procedures on the fMRI results from the standard analysis framework. For the visuomotor task, the neural response to each trial was modeled as an event of 0.5-s duration. For the hyperventilation condition, a boxcar with 25-s duration modeled the activation related to volitional inhalation/exhalation. Similarly, both the onset and offset timing of breath holding were used to model the time-locked neural activity to respiratory control. The canonical hemodynamic response function was convolved to the model timeseries to create the regressors of interest. All activation maps were thresholded at $p = 0.05$ after correcting for multiple comparisons, using family-wise error across the whole brain (Poline et al., 1997).

2.4.3 Relative BOLD transit time

Fig. 3A illustrates the method. This analysis was performed on data from Experiment 1, acquired at a short TR of 0.5 s. The lag structure consisted of a lag map and the set of timeseries averaged over the voxels with the same phase. This structure implicitly represents the propagation of the sLFO phase along the vessels. The phase is expected to cross the boundary between adjacent regions of the vascular tree every 0.5 s, the lag tracking step, on average. However, if there is variation in propagation velocity, there would be deviation of the instantaneous phase difference from 0.5 between neighboring regions. Here, the phase difference is supposed to reflect the time the blood requires to cross the boundary between the voxel groups.

To test this supposition, the phase difference fluctuation was calculated from each of the 16 pairs of seeds corresponding to lags of -4 to +4 s at 0.5-s intervals. Owing to the broad frequency range of the fluctuations of interest, we considered that a smooth sliding window algorithm was appropriate instead of analytic methods (window length = 30 s, Kaiser window with a parameter beta of 4). The region timeseries were resampled to a 0.02-s resolution to capture minute phase difference fluctuation (4%) from 0.5 s. Instantaneous phase differences from each pair of seeds were averaged over respiratory task events and divided by 0.5 to obtain the time course of the rBTT. The rBTTs from the 16 pairs of neighboring regions were then averaged to obtain the regional or global rBTT. According to this model, the inverse of the rBTT corresponded to the instantaneous relative velocity, as the rBTT should reflect the average time the blood requires to traverse fixed distances because the lag map is determined by the baseline average velocity.

2.4.4 Multi-echo combination

For Experiment 2, involving multi-echo acquisition, S_0 and T2* datasets were created by a simple estimation, following earlier work (Posse et al., 1999; Yen et al., 2017). We assumed a single compartment monoexponential decay of the MR signal as follows:

$$\boldsymbol{S(TE) = S_0\ exp(-TE/T_2{}^*)} \qquad [4],$$

where T2* and S_0 were calculated for each TR as follows (Kundu et al., 2012; Posse et al., 1999):

$$\boldsymbol{T_2{}^* = (TE2 - TE1)/\ln\,(S_1/S_2)} \qquad [5] \text{ and}$$

$$\boldsymbol{S_0 = S_1{}^{TE2/(TE2-TE1)}/S_2{}^{TE1/(TE2-TE1)}} \qquad [6],$$

where S_1 and S_2 are the acquired signals at TE1 and TE2, respectively. Negative values or T2* exceeding 100 ms were considered as noise and were ignored. All four datasets (S_0, S_1, S_2 or BOLD, and T2*) were entered into the same analysis pipeline used for Experiment 1 but taking the different TR of 1.3 s into account. The following analyses were performed on a resampled time course at a TR of 0.5 s.

The interaction between the signal component and vascular anatomy was examined by extracting the signal timeseries from the inlet, center, and outlet parts of the vascular tree, based on the individual lag map created from the BOLD (i.e., TE2) dataset. By exploiting the longer lag tracking range (± 7 s) than the one used in the rBTT analysis in Experiment 1, the center region in this analysis covered a wider range (± 2.5 s). Using the JMP12 Software (SAS Institute, Cary, NC), the

magnitude and phase of the regional signals were analyzed by repeated-measures ANOVA followed by post hoc analysis, using Tukey's honestly significant difference (HSD) test. Statistical significance was assumed for $p < 0.05$. Additional analyses were performed to examine the signal components, including a region-of-interest analysis and an SPM analysis of respiration phase-related small S_0 fluctuation.

3 Results

The average root mean square of head motion measured as the framewise displacement, i.e., the shift in the position of the brain in one volume compared to the previous volume, was 0.039 ± 0.007 mm (mean ± standard deviation over subject) for Experiment 1, with a maximum displacement of 0.37 ± 0.18 mm, and 0.034 ± 0.015 mm for Experiment 2, with a maximum of 0.24 ± 0.12 mm (Van Dijk et al., 2012).

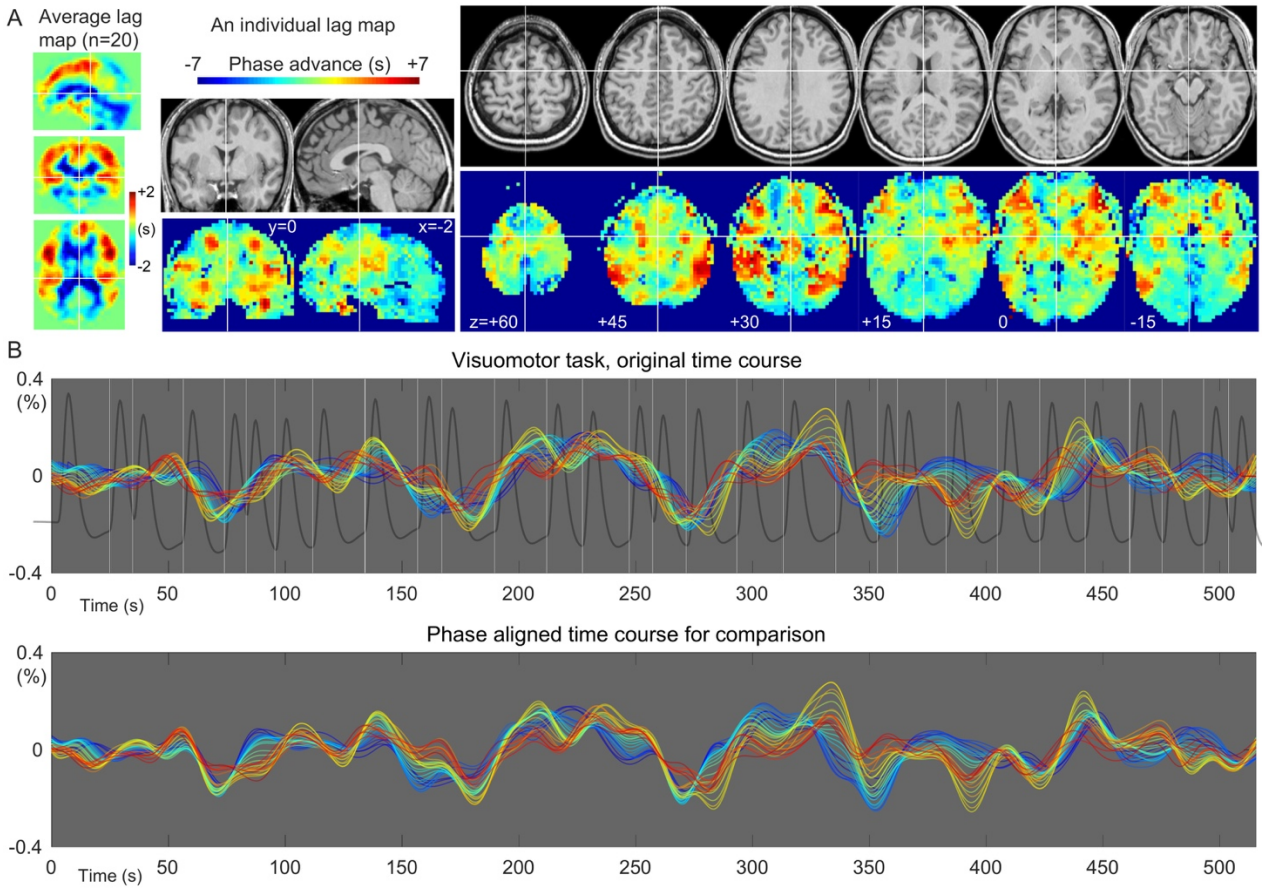

Fig. 2. Representative spatial and temporal profiles of the BOLD lag structure. (A) Lag map created by tracking the BOLD low-frequency oscillation (LFO) phase up to 7 s toward both up- and downstream. Group average map reflects the gross vascular anatomy with the early phase (positive values) distributed in the middle cerebral artery territories. The individual map reflects the vascular structure more precisely. (B) Seed time courses updated at each step (0.5 s) of the recursive lag tracking procedure, representing the temporal aspect of the lag structure. The warm-colored traces with advanced phase originate from the voxels with the same colors in the

lag map, corresponding to the inlet or arterial side of the vasculature. A gradual change in the temporal profile is noted on top of the slow component, which is stable across regions. The white vertical lines indicate the timing of the visuomotor task, whose NVC was modeled by the hemodynamic response function (dark gray trace). The detected LFO was poorly correlated with the task-related fluctuation of neuronal origin (see main text).

Fig. 2A shows the average and an individual BOLD lag map during the sparse visuomotor task. Warm colors indicate a positive travel time from those voxels to the phase of the global LFO, signifying that the voxels are considered "upstream." Most brain voxels fell into the -4 to +4 s range (mean ± SD, 93.8 ± 2.9%). The recursively defined seed time courses are shown in **Fig. 2B** with warm colors indicating averaged timeseries from the upstream voxels. This time course of the lag structure was poorly correlated with the visuomotor task (white vertical lines) or the evoked NVC response (trace in dark gray), indicating a dominant contribution of sLFO. This was confirmed by the correlation coefficient between the global mean signal and the modeled response that was not significantly different from zero (0.0265 ± 0.140, mean and SD over 20 participants), although still slightly positive in some subjects and its regression affected the activation maps (see section 3.2). In addition to the constant phase shift across regions, the lag structure time courses presented minute fluctuations of the phase difference (i.e., the temporal relationship between the lines) over time.

3.1 Flow velocity information in the instantaneous phase

A transient change in propagation velocity of the low-frequency phase, obtained as the inverse of the global rBTT, was found in response to the respiratory challenges. **Fig. 3B** shows the stacked histograms of distribution of instantaneous phase difference measured by the moving window analysis. This instantaneous phase difference (in s) is interpreted as the time the blood required to move over a unit distance that requires 0.5 s on average. The time courses are presented in **Fig. 3C**. After approximately 10 s of delay, increase and decrease of the BOLD signal was found during breath holding and hyperventilation, respectively (arrows). This delay in the BOLD response by autoregulation is consistent with earlier work (Murphy et al., 2011).

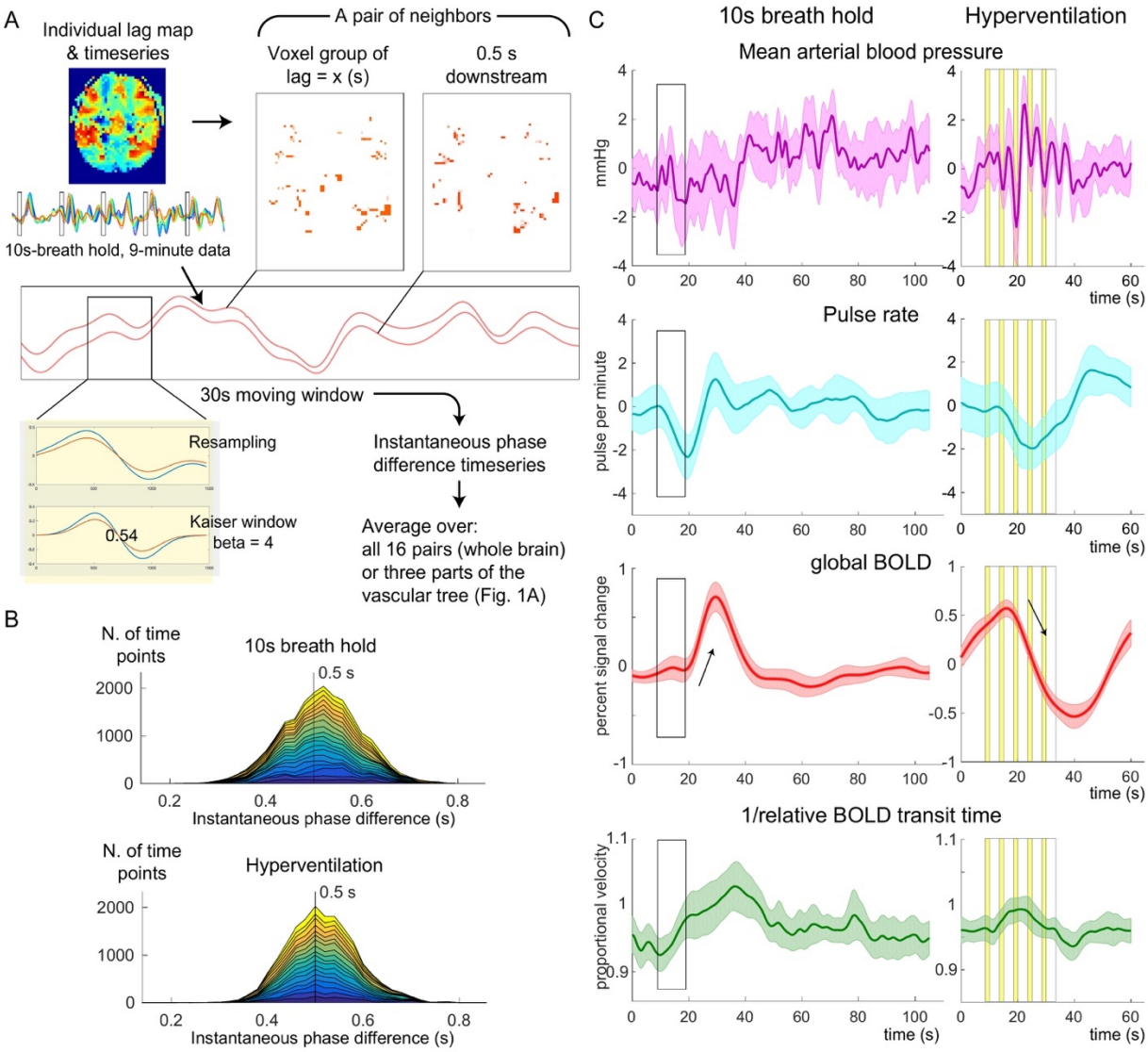

Fig. 3. Measurement of relative bold transit time (rBTT). (A) Schematic illustration of the analysis. For each pair of voxel groups representing neighboring regions of the vascular tree, the two average timeseries were fed into a moving window analysis of instantaneous phase difference. (B) Time point histograms of the instantaneous phase difference averaged over 16 pairs of neighboring regions in the lag structure. Twenty subjects are stacked. Deviation of the phase difference from 0.5 s reflects a fluctuation of the flow velocity, although the slight shift of the peak is observed in the breath hold data presumably due to the effect of windowing. (C) Response to the respiratory challenges of the physiological recordings, the raw BOLD signal, and inverse of the rBTT that can be interpreted as relative velocity. Thin arrows indicate the autoregulatory response of the raw BOLD signal. The five cycles of volitional breathing for hyperventilation are indicated with yellow bands representing the inspiration phase. Shaded areas indicate the 95% confidence interval of the mean across subjects.

The temporal profile of the instantaneous velocity (green curves) was roughly in phase with the global BOLD response but had different onset and peak timings, indicating the different physiological bases. To evaluate the relationship of this phenomenon with the vascular structure,

375 the inlet, center, and outlet regions were separately analyzed (**Fig. 4**). In both respiratory
376 challenges, there was a clear asymmetry over the vasculature, with pronounced velocity responses
377 in the inlet region, despite similar BOLD response profiles. In the outlet region, or the venous side of
378 the vasculature, a velocity response was not clearly found.

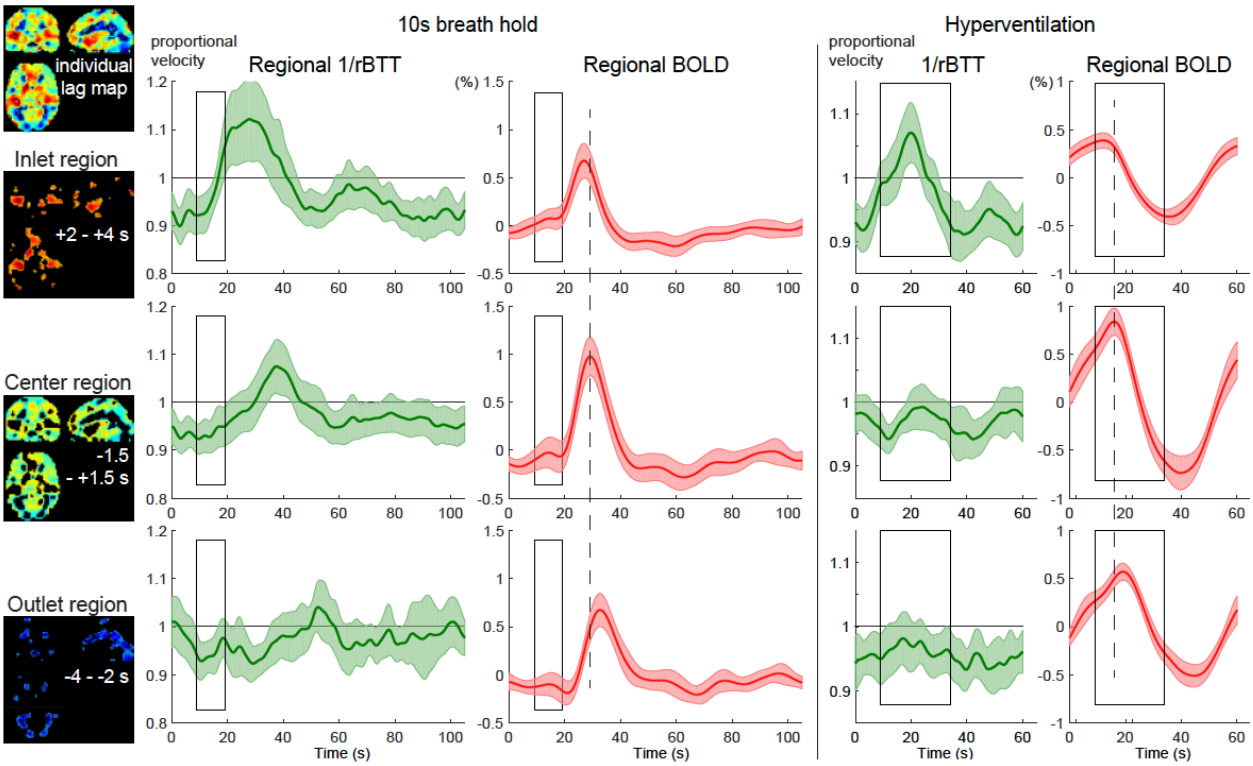

379

380 **Fig. 4.** Autoregulatory responses to respiratory challenges in the three vascular regions, using
381 the same conventions as in **Fig. 3**. The inlet (arterial side), center, and outlet (venous side) of the
382 parenchymal vasculature were defined for each subject, using the lag map created from the
383 session data per se. The relative changes in propagation velocity were detected as the inverse of
384 instantaneous transit time deviation from 0.5 s (rBTT), since the lag mapping was performed at
385 0.5-s steps. The BOLD signal time courses present different peak latencies for the three regions
386 (broken lines are aligned to the center region peak), directly reflecting the lag structure, but with
387 similar profiles, ruling out its effects on the rBTT measurement. Shaded regions represent the
388 95% confidence intervals (N = 20).

389

390 **3.2 Effect of deperfusioning on the detection of NVC**

391 Removal of the whole lag structure exhibited unique effects on the fMRI analysis. While the mean
392 and standard deviation images from the individual activation maps showed similar spatial
393 distribution, all procedures reduced the activation level compared to the result from removing only
394 the motion-related variances (**Fig. 5**). However, after the deperfusioning procedure, primary motor
395 cortex activation was detected by decreased interindividual variances (black circles). The effect of

these procedures was not uniform between the respiratory challenges (**Fig. 6**), but some interpretable clusters were selectively captured by the "deperfusioned" signals despite the reduced cluster number. For example, the so-called laryngeal motor cortices were successfully detected at the onset and offset of the 10-s breath-holding (Kumar et al., 2016). In the hyperventilation condition, we observed bilateral recruitment of the putamen. This is consistent with reports using optimized acquisition techniques (Dresel et al., 2005; Pattinson et al., 2009), supported by anatomical (Simonyan and Jürgens, 2003), as well as electrophysiological (Radna and MacLean, 1981) studies. A premotor peak found at coordinates [+56, 0, 40] was also very close to the reported activation site for volitional respiration (McKay et al., 2008).

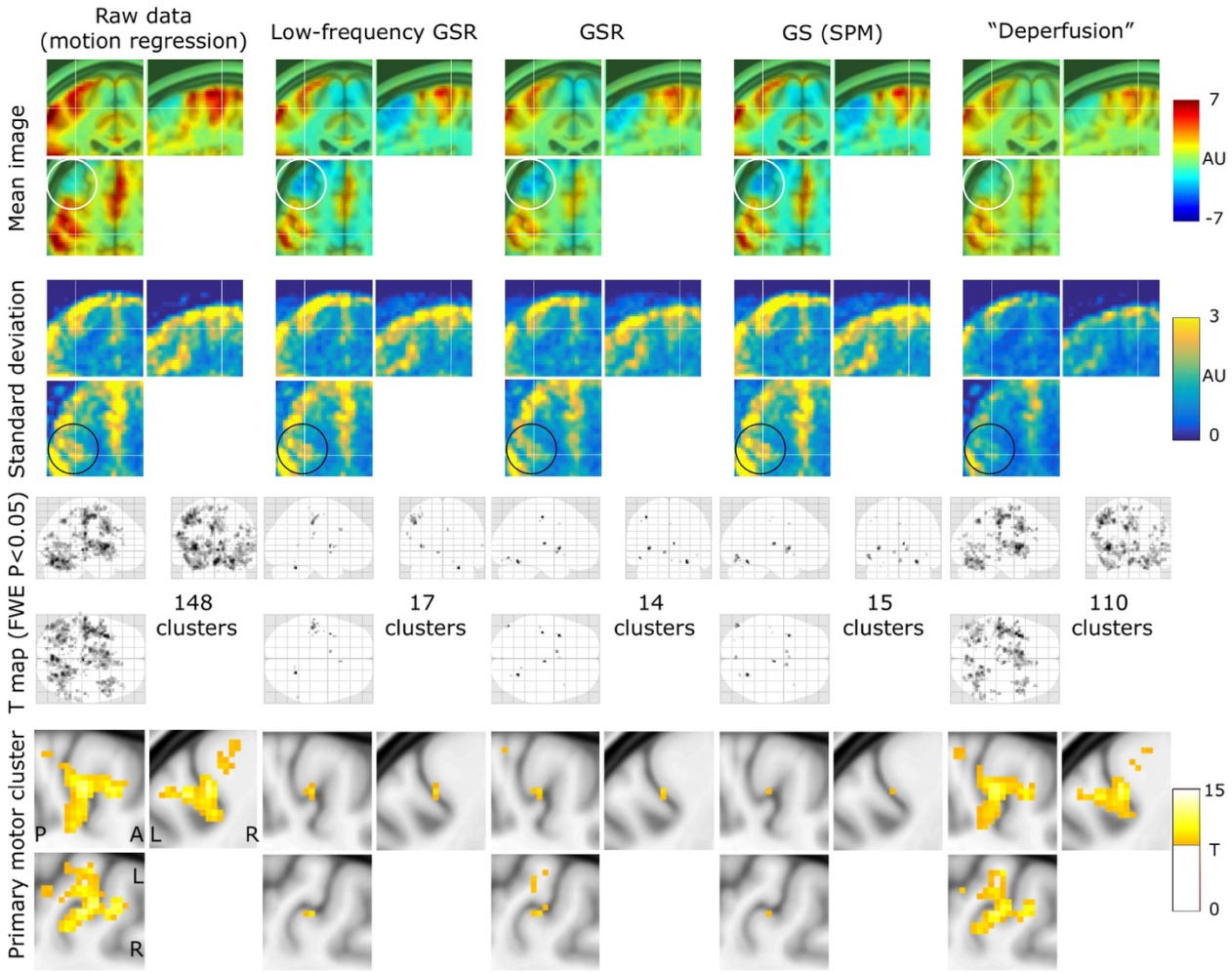

Fig. 5. Effect of the denoising procedures on the detection of neurovascular coupling during the visuomotor task. Mean and standard deviation maps from 20 individual activation maps (contrast images) illustrate the spurious negative responses by the global-signal based methods (white circle) and the reduced between-subject variation by the lag structure removal or deperfusioning (black circle). Activation maps were thresholded at p = 0.05, corrected for FWE of multiple comparisons over the entire brain, and zoomed in to show the "hand-knob" of the left primary sensorimotor cortex. FWE, family-wise error corrected.

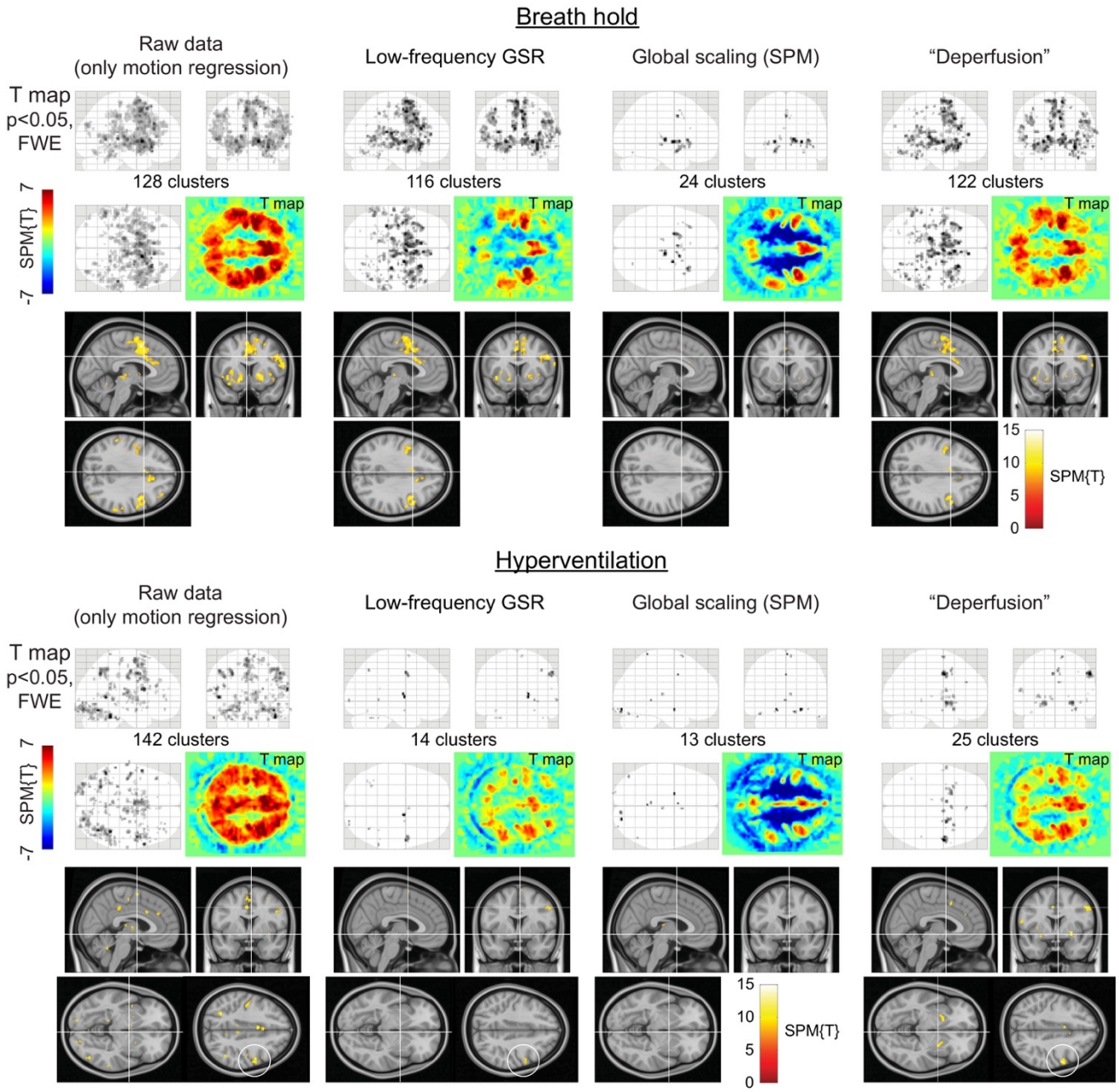

Fig. 6. SPM results of the respiratory challenges. Color panels show un-thresholded t map slices at the height of the laryngeal motor cortex (z = 35) (Kumar et al., 2016), revealing spurious negative responses (cool colors) after global signal removal but not after the deperfusioning procedure. In the hyperventilation condition, the "deperfusioned" data revealed clusters in the bilateral putamen and premotor cortex (white circle), consistently with the findings of earlier reports.

Voxel histograms from the group SPMs showed clear leftward shifts by the global signal removal, indicating spurious deactivations (**Fig. 7**). The correlation of the neuronal response with the global signal was small, as described above, but it varied across subjects and tended to be positive. This

trace of NVC may have created the spurious deactivation after regression. Notably, this effect was very weak after deperfusioning across all three conditions, despite a large amount of variance removed by the procedure. This finding is in agreement with the results of earlier work on resting-state fMRI (Erdoğan et al., 2016).

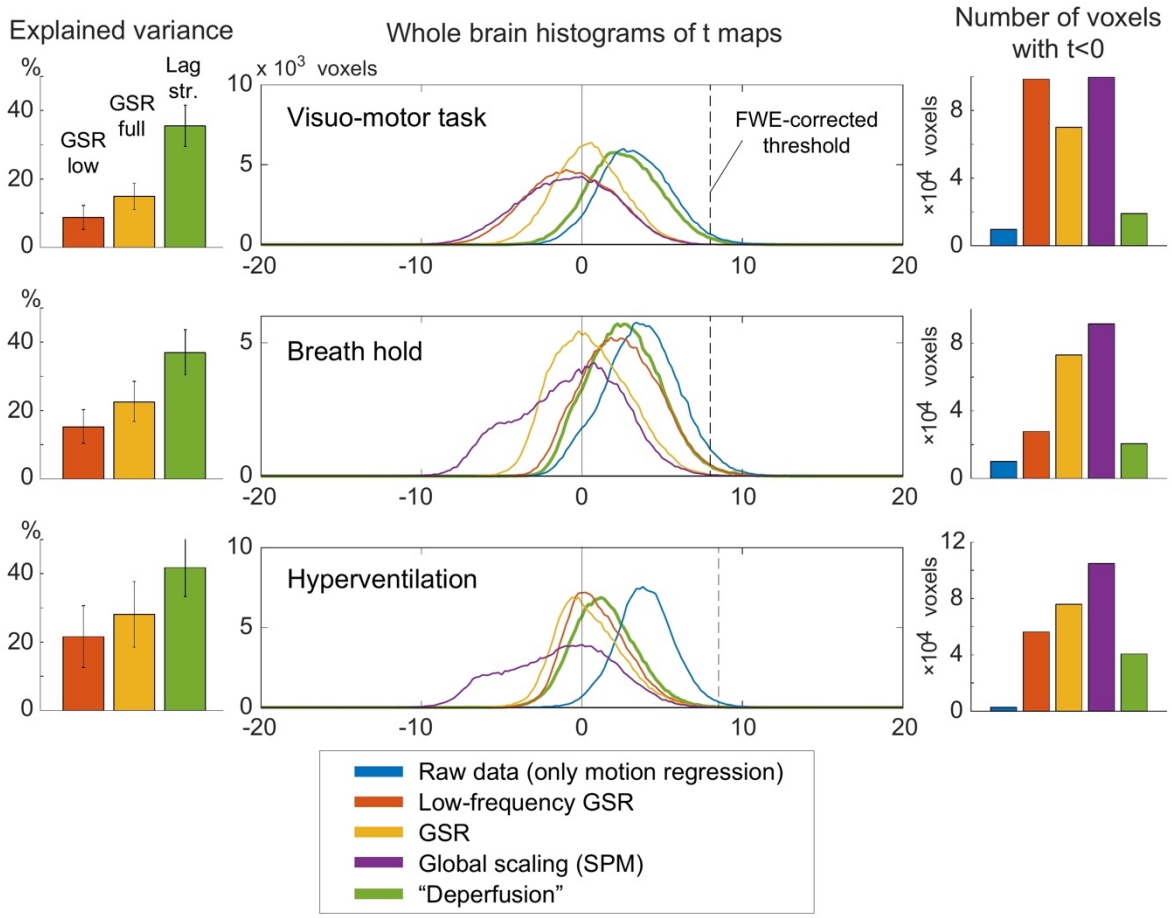

Fig. 7. Effect of preprocessing on group SPMs. Removal of the lag structure or deperfusioningresulted in greatest reduction of the signal variance under all three tasks (left panels). Nevertheless, the spurious negative task responses were attenuated in comparison to the removal of global fluctuation (middle and right panels). Error bars indicate the standard deviation. The vertical broken line in the histogram indicates the statistical height threshold of p = 0.05, corrected for multiple comparisons by family-wise error rate. GSR, global signal regression.

3.3 MR signal components of the lag structure

As depicted in **Figure 8**, the percent signal change of the low-frequency seed timeseries, or the lag structure amplitude, revealed a clear T2*-dependence with a significant reduction of amplitude in the outlet, i.e., the venous side (post hoc Tukey's HSD between T2* signals from the inlet and outlet

441 regions, following a repeated-measures ANOVA). This finding replicates a previous observation in
442 the raw BOLD signal (Aso et al., 2017a).

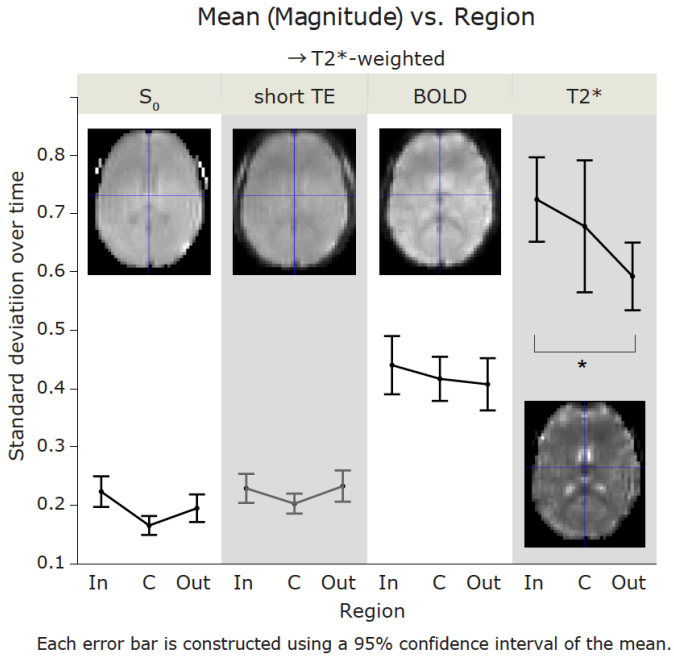

443

444 **Fig. 8.** Standard deviation of the percent signal change as a measure of signal magnitude after
445 bandpass filtering. No main effect of vascular region was observed by repeated-measures
446 ANOVA, but the T2* magnitude was significantly different between the inlet and outlet or
447 arterial and venous sides ($p < 0.05$, Tukey HSD). The short-TE image was not included in the
448 analysis to avoid data redundancy.

449

450 In lag maps from the three T2*-weighted images, we noted some effect of the respiratory
451 challenges, but the gross cerebral vascular structure was preserved across tasks; the periventricular
452 regions and major venous sinuses were uniformly found downstream (i.e., with negative arrival
453 time) of the global signal phase, while the cortical territory of the middle cerebral arteries
454 presented earlier arrival (**Fig. 9A**). Only the S_0 image presented a different lag structure according to
455 the image correlation (**Fig. 9A**, right panels).

456 Temporal analysis of the signal components revealed significant main effects of both region [F
457 $(2,532) = 16.877$, $p < 10^{-6}$] and T2* weighting [F $(2,532) = 280.786$, $p < 10^{-6}$] (**Supp. Fig. 1A**). The S_0
458 timeseries failed to show a correlation with the T2*-weighted signals, but the z-value in the inlet,
459 i.e., the arterial side, differed significantly from other regions ($p < 0.05$, Tukey's HSD). A region
460 effect was also found for phase relationships (**Supp. Fig. 1B**). Again, the main effects for both region
461 [F $(2,532) = 27.548$, $p < 10^{-6}$] and T2* weighting [F $(2,532) = 44.679$, $p < 10^{-6}$], as well as their
462 interaction [F $(4,532) = 24.902$, $p < 10^{-6}$], were significant. The phase of the short TE signal, which is
463 less T2*-weighted than is BOLD, gradually advanced, finally showing a phase lead in the outlet
464 region. This alone suggests varying relationships between the two components across vascular

regions. These signal phase dissociations within regions are displayed in **Supp. Fig. 1C**. Significant differences among the three T2*-weighted signals were also found after the post-hoc test ($p < 0.05$). The signal-region interaction was evident in the signal response to the respiratory challenges shown in **Fig. 9B**. The traces contain higher frequency components, which were eliminated for lag mapping. In contrast to the changes in T2* responses for both phase and magnitude, the S_0 component was stable across vascular regions.

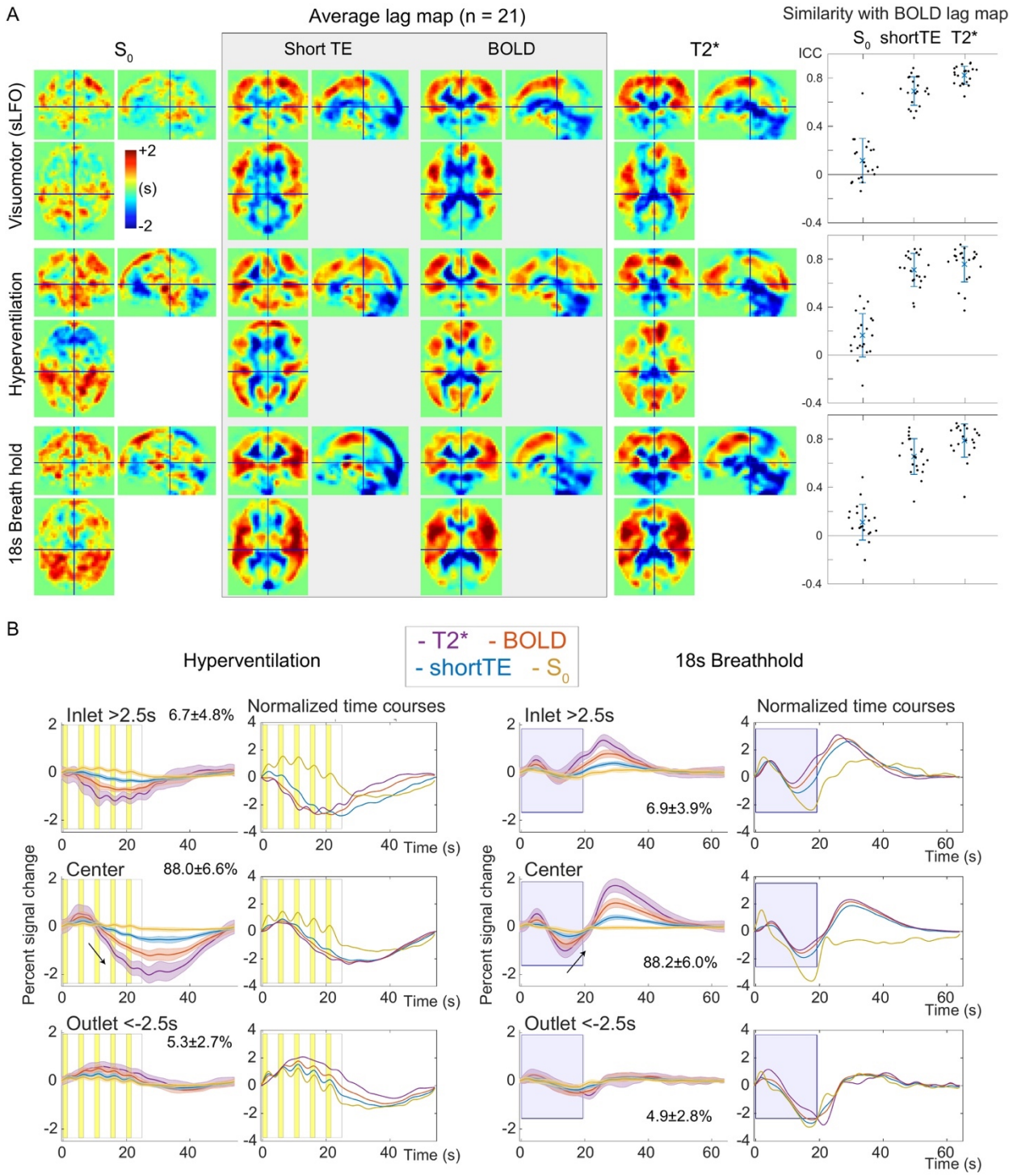

472 **Fig. 9.** Analysis of signal components and the lag structure. *A*, S_0 and T2* signals were
473 interpolated based on multi-echo acquisition at short and typical echo times for BOLD fMRI. The
474 lag map created from the S_0 image shows a unique structure but fails to reflect the arterial and
475 venous structures that are consistently found in the BOLD lag map. Using the T2*-weighted
476 signals, the lag map changes upon respiratory challenges, which should primarily reflect the
477 modification of the perfusion pattern; however, an interaction with the signal component is not
478 excluded. The right panels show intraclass correlation coefficients as a quantitative measure of
479 within-subject image similarity with the BOLD lag map, with error bars indicating 95%
480 confidence intervals. *B*, Temporal profiles from the three vascular regions indicate absence of
481 region effect in the S_0 signal, suggesting a globally uniform mechanism underlying the S_0
482 response.

483

484 To further investigate the signal origin, we extracted the response in the motor/premotor area
485 activation peak, where NVC was expected to dominate (**Supp. Fig. 2A**). For this analysis, the group
486 activation map from Experiment 1 was used to define the regions-of-interest in order to avoid bias.
487 We found high-frequency components dominating the S_0 responses in comparison to the responses
488 from larger regions shown in **Figure 9B**. During hyperventilation, it presented respiratory phase-
489 related fluctuations, with a signal decrease initiated by inhalation and followed by a positive
490 deflection during exhalation. The T2* signal also exhibited small fluctuations but with a different
491 phase, possibly dominated by the NVC component.

492 We conducted an additional analysis for this fast respiration-related non-BOLD component. The
493 spatial distribution of this response is shown in **Supp. Fig. 2B**. Interestingly, there was a clear
494 anterior-posterior segmentation of response polarity, with the posterior regions presenting the
495 opposite phase of this fast S_0 deflection by respiratory maneuver. Some additional symmetrical
496 structures were found in deep-brain regions, near the deep middle cerebral and inferior ventricular
497 veins, implying a unique vascular involvement. Importantly, this spatial pattern was not that of a
498 typical motion artifacts that can accompany volitional respiration in spite of the careful instruction.

499 Finally, **Supp. Fig. 2C** shows the data from a subset of participants, obtained using a different
500 TR/flip-angle setting to manipulate the inflow effect. The T2* response was smaller than that shown
501 in the panel **2A**, presumably due to the short TR. The different TR also contributed to the rich high-
502 frequency components by the fast sampling rate. The slow S_0 change was also diminished, but the
503 respiration-related fast component was relatively preserved suggesting absence of a strong inflow
504 effect.

505 **4 Discussion**

506 The principal findings of this study are summarized as follows. First, based on the instantaneous
507 phase difference within the BOLD lag structure, we observed a trace of blood flow velocity change

508 selectively in the inlet region of the vasculature. Next, the complete elimination of the lag structure
509 reduced interindividual variance and spurious deactivation, supporting our hypothesis that NVC
510 could be observed more specifically by this deperfusioning procedure. Finally, the lag structures in
511 the S_0 (or non-BOLD) component did not correlate with that from T2*, either spatially or temporally.
512 We also found a vascular region-dependent change in the T2* LFO, with a decreased amplitude in
513 the venous side, in contrast to the S_0 response that remained constant in both amplitude and
514 phase. The S_0 component exhibited a unique brain region-dependent response to the respiratory
515 phase, suggesting that certain perfusion parameters are specifically contributing to this component,
516 but not the perfusion timing. Overall, the BOLD low-frequency phase behaved as a deoxy Hb-based
517 virtual contrast agent in the present data, leaving a global, but separable noise component for the
518 fMRI analysis.

519 The observation that the velocity on the arterial side exhibits changes alongside respiratory
520 variations is consistent with the findings of previous reports using transcranial Doppler
521 ultrasonography (Malatino et al., 1992; Poulin et al., 1996). During the initial whole-brain CBV
522 increase in response to autoregulatory vasodilation, a sole increase in the inflow should first occur
523 to meet the volume demand. It is reasonable that this effect is absent in the outlet, i.e., the venous
524 side of the gross vasculature, as observed in the current study. The low-frequency phase hence
525 appears to directly reflect the perfusion.

526 This result is compatible with the model that the BOLD lag structure is derived from an axial non-
527 uniformity in the vessels, already present in the inflow (Tong et al., 2018). The diminished
528 magnitude observed in the outlet side of the vasculature may also suggest a distinct origin of the lag
529 structure, other than NVC which can create a threefold larger response in the draining vessel (Krings
530 et al., 1999). If the source of this axial variation creating the sLFO is systemic, i.e., originating from
531 the autonomic loops, mediated by peripheral baro- or chemoreceptors, there may be no direct link
532 with local neural activity. In this work, we focused on non-neuronal mechanisms to account for the
533 BOLD lag structure to the extent possible, in the hope that it may ultimately help achieve a better
534 understanding and modeling of the fMRI signal.

535 **4.1 Source of BOLD LFO signals**

536 Previous studies on sLFO in Hb-based brain signals have reported that both Hb species fluctuate,
537 but with varying phase difference that is selectively found in the brain (Obrig et al., 2000;
538 Rayshubskiy et al., 2014; Tgavalekos et al., 2016). The observed fluctuations of total Hb density have
539 been linked to CBV changes (Boas and Dale, 2005; Kennerley et al., 2005; Kim and Ogawa, 2012),
540 but interpretations for that of deoxy-Hb have rarely been provided. Only one series of studies by
541 Fantini and others directly addressed the possible axial variation of blood content including oxygen
542 saturation (Fantini, 2014). Rayshubskiy and colleagues reported, in their important human
543 intraoperative study, the synchronized sLFO of vasomotion and Hb using near-infrared optical

544 signals (Rayshubskiy et al., 2014). Although diameter changes in deep parenchymal vessels may not
545 range in the tens of a percent, as observed for superficial vessels, the correlation of vasomotion to
546 Hb sLFO appears to be established. However, it remains to be clarified whether an equivalent
547 vasomotion exists in the non-arterial vessels. Besides, vasomotion may itself create axial variation
548 of the blood content, such as Hct. Vasomotion was originally found as an active diameter change in
549 the precapillary vessels, driving local velocity fluctuations, termed "flowmotion" (Intaglietta, 1990).
550 This flowmotion can reportedly accompany the fluctuation of local Hct that is known to change with
551 vessel diameter (Fagrell et al., 1980; Hudetz et al., 1999). Another possible source for the deoxy-Hb
552 fluctuations could be a change in SaO2 that ranges from 94–98% in the artery (Collins et al., 2015b;
553 Intaglietta et al., 1996). For example, the respiration-related BOLD signal component is supposed to
554 be mediated by blood CO_2 level and pH, which also shift the oxygen dissociation curve (Birn et al.,
555 2006; Chang and Glover, 2009b). These parameters are considered to fluctuate in the blood as part
556 of the autonomic loop. As mentioned above, the phase difference between the two Hb species
557 remains to be elucidated (Sassaroli et al., 2012), but such uncoupled axial variations observed in
558 different settings may substantiate an unstable deoxy-Hb supply in most brain tissues. Such a signal
559 component would have escaped detection by trial averaging in NVC studies, as it is uncoupled to
560 neural activity.

561 A signal origin intrinsic to the flowing blood may be thus required, as suggested by Tong and
562 colleagues, to explain the constant phase difference among signals from different body parts (Tong
563 et al., 2012, 2017). In the literature, an axial variation of the Hct in the brain has indeed been
564 suggested, in relation to both NVC (Chen and Pike, 2009; Kleinschmidt et al., 1996; Siegel et al.,
565 2003) and sLFOs (Fagrell et al., 1980; Mayhew et al., 1996). Furthermore, the reduction in T2* LFO
566 amplitude in the venous side can be explained by the high tissue deoxy-Hb density, which probably
567 diminishes the proportional effect of intrinsic deoxy-Hb fluctuations, unless the oxygen
568 consumption is completely coupled to this variation. Importantly, temporal dispersion alone would
569 not fully account for the amplitude reduction, as it was only found in the venous side, despite the
570 fact that the lag structure was tracked both up- and downstream from the global signal phase.
571 These results provide good contrast with the stable S_0 response, reflecting its insensitivity to oxygen
572 saturation. Although it would be too challenging to incorporate complex rheological parameters
573 into the model, a reconsideration of the constant deoxy-Hb assumption may help better isolate the
574 NVC from the BOLD signal (Uludağ and Blinder, 2018).

575 In the hyperventilation condition, we observed a fast response to each ventilation cycle,
576 accompanying blood pressure change. Although the effect of respiratory movement cannot be fully
577 excluded, the spatial pattern in **Supplementary Figure 2B** is not that of a typical motion artifact
578 centered on the brain surface (Krings et al., 2001). In healthy subjects, inhalation increases systemic
579 venous return through decreased intrathoracic pressure, causing elevation of the cardiac output
580 with some delay. In contrast, exhalation is considered to cause CBV increase through elevated
581 cerebral venous pressure. To our knowledge, the timing order of these events has not been studied

582 at the precision of the current data, and further studies are needed to determine the source of this
583 S_0 fluctuation (Yen et al., 2017). The only available clue is the spatial distribution, such as the
584 interesting anterior-posterior segmentation (resembling the unique "S_0 lag structure" in **Fig. 9a**) or
585 the symmetrical pattern in the deep brain structures. At least, some mechanical effect of the
586 respiratory act likely exists, causing this spatially-heterogeneous S_0 deflection.

587 **4.2 Lag structure as noise**

588 As the global signal should ideally be the sum of all variations caused by NVC, its elimination by GSR
589 or rendering it constant by global mean scaling has been considered to negatively bias the results
590 (Caballero-Gaudes and Reynolds, 2017). However, as noted by Aguirre and others, there are cases
591 where GSR yields "preferable" results that are easy to interpret even in the absence of global noise
592 such as motion artifacts (Aguirre et al., 1998). The rise in popularity of rs-fMRI since 2005 has led to
593 this issue resurfacing in a different form. A variation in GSR, in which the timeseries extracted from
594 a set of regions-of-interest (whole brain, white matter, and cerebrospinal fluid) are removed, has
595 become a *de facto* standard. It is indeed computationally closer to our deperfusioning in that the
596 regional phase difference is somehow tolerated. However, because this practice lacked strong
597 theoretical background (Chang et al., 2009; Liu et al., 2017), currently, the identification and
598 elimination of bodily movements and physiological noise are more widely recommended. There are
599 various approaches to this end, such as simultaneous physiological measurements (Chang and
600 Glover, 2009a), as well as data-driven methods that only use fMRI data (Smith et al., 2013).
601 However, the unavailability of objective criteria for distinguishing neural activity from noise
602 components remains an issue (Salimi-Khorshidi et al., 2014).

603 In the present study, the lag structure was treated as a broadly-distributed structured noise for
604 fMRI. It can actually be substantially eliminated by sophisticated denoising techniques (Aso et al.,
605 2017a). The specificity of lag mapping in isolating information on a purely vascular origin remains,
606 however, unknown. For example, measurement of velocity changes critically depends on a recursive
607 lag-tracking method, which incorporates the gradual change in LFO over regions (Tong and
608 Frederick, 2014). Adaptation for changes in the waveform that may arise from different paths of the
609 blood is not only theoretically plausible, but was demonstrated to increase the reproducibility of the
610 lag (Aso et al., 2017a). However, as the changes in waveform reflect any fluctuation originating
611 either from the vascular anatomy or NVC, removing the whole lag structure may lead to type II
612 errors in the fMRI results. The favorable impacts of the deperfusioning procedure that we observed
613 on the fMRI results are clearly insufficient to prove the advantage of this technique and require
614 further confirmation.

615 Importantly, the detection of the lag structure itself is dependent on data quality and affected by
616 body movements. This would be the case when a significant head movement results in a
617 synchronized deflection that exceeds the LFO amplitude, thus obscuring the phase difference across

voxels. However, it can be also questioned if the correlational structure of neural activity is reliably detected from such motion-contaminated data. This is because, in general, NVC should have a lower spatial extent and signal magnitude, which requires time-locked averaging to detect (Power et al., 2012). In turn, successful tracking of a lag structure may even be considered as evidence of "clean" data. Thus, the elimination of this identified lag structure can be a relatively straightforward approach to reduce structured physiological noise (Caballero-Gaudes and Reynolds, 2017).

In conclusion, by investigating various aspects of the BOLD sLFO, we compiled supporting evidence for a component intrinsic to flowing blood that has been a focus of interest in earlier works (Tong et al., 2017). To establish a framework by which the fMRI signal can be fully modeled, more detailed characterization of the lag structure as part of the "global noise" is needed (Glasser et al., 2018).

5 Conflict of Interest

The authors declare that the research was conducted in the absence of any commercial or financial relationships that could be construed as a potential conflict of interest.

6 Author Contributions

All authors provided approval of the final version of the manuscript to be published. TA contributed to concept and design of this research, data analysis and interpretation, and drafting of the manuscript. SU contributed to data acquisition and drafting of the manuscript. SU, HF, and TM contributed to data interpretation and review of the final draft.

7 Funding

This study was supported by Grants-in-Aid for Scientific Research on Innovative Areas (JP15H05875) to T.A. and JP16H06395 and JP16H06397 to T.M. from the Japan Society for the Promotion of Science.

8 Acknowledgments

We would like to thank Editage (www.editage.jp) for English language editing.

9 Data Availability Statement

The datasets analyzed for this study can be provided upon request.

10 References

Aguirre, G. K., Zarahn, E., and D'Esposito, M. (1998). The inferential impact of global signal covariates in functional neuroimaging analyses. *NeuroImage* 8, 302–6. doi:10.1006/nimg.1998.0367.

Amemiya, S., Kunimatsu, A., Saito, N., and Ohtomo, K. (2013). Cerebral Hemodynamic Impairment: Assessment with Resting-State Functional MR Imaging. *Radiology* 270, 1–8. doi:10.1148/radiol.13130982.

Amemiya, S., Takao, H., Hanaoka, S., and Ohtomo, K. (2016). Global and structured waves of rs-fMRI signal identified as putative propagation of spontaneous neural activity. *NeuroImage* 133, 331–340. doi:10.1016/j.neuroimage.2016.03.033.

An, H., and Lin, W. (2002). Cerebral oxygen extraction fraction and cerebral venous blood volume measurements using MRI: Effects of magnetic field variation. *Magnetic Resonance in Medicine* 47, 958–966. doi:10.1002/mrm.10148.

Anderson, J. S., Druzgal, T. J., Lopez-Larson, M., Jeong, E., Desai, K., and Yurgelun-Todd, D. (2011). Network anticorrelations, global regression, and phase-shifted soft tissue correction. *Human brain mapping* 32, 919–34. doi:10.1002/hbm.21079.

Aso, T., Jiang, G., Urayama, S., and Fukuyama, H. (2017a). A Resilient, Non-neuronal Source of the Spatiotemporal Lag Structure Detected by BOLD Signal-Based Blood Flow Tracking. *Frontiers in Neuroscience* 11, 256. doi:10.3389/fnins.2017.00256.

Aso, T., Urayama, S., and Fukuyama, H. (2017b). Temporal variation of cerebrovascular transit time measured by BOLD-based time lag mapping. in *Proceedings of the 25rd Annual Meeting of ISMRM* (Honolulu).

Birn, R. M., Diamond, J. B., Smith, M. a., and Bandettini, P. a. (2006). Separating respiratory-variation-related fluctuations from neuronal-activity-related fluctuations in fMRI. *NeuroImage* 31, 1536–1548. doi:10.1016/j.neuroimage.2006.02.048.

Birn, R. M., Murphy, K., and Bandettini, P. A. (2008). The effect of respiration variations on independent component analysis results of resting state functional connectivity. *Human Brain Mapping* 29, 740–750. doi:10.1002/hbm.20577.

Blockley, N. P., Driver, I. D., Francis, S. T., Fisher, J. A., and Gowland, P. A. (2011). An improved method for acquiring cerebrovascular reactivity maps. *Magnetic Resonance in Medicine* 65, 1278–1286. doi:10.1002/mrm.22719.

Boas, D. A., and Dale, A. M. (2005). Simulation study of magnetic resonance imaging–guided cortically constrained diffuse optical tomography of human brain function. *Applied Optics* 44, 1957. doi:10.1364/AO.44.001957.

Buxton, R. B. (2012). Dynamic models of BOLD contrast. *NeuroImage* 62, 953–61. doi:10.1016/j.neuroimage.2012.01.012.

Byrge, L., and Kennedy, D. P. (2018). Identifying and characterizing systematic temporally-lagged BOLD artifacts. *NeuroImage* 171, 376–392. doi:10.1016/j.neuroimage.2017.12.082.

Caballero-Gaudes, C., and Reynolds, R. C. (2017). Methods for cleaning the BOLD fMRI signal. *NeuroImage* 154, 128–149. doi:10.1016/j.neuroimage.2016.12.018.

Chang, C., Cunningham, J. P., and Glover, G. H. (2009). Influence of heart rate on the BOLD signal: The cardiac response function. *NeuroImage* 44, 857–869. doi:10.1016/j.neuroimage.2008.09.029.

Chang, C., and Glover, G. H. (2009a). Effects of model-based physiological noise correction on default mode network anti-correlations and correlations. *NeuroImage* 47, 1448–59. doi:10.1016/j.neuroimage.2009.05.012.

Chang, C., and Glover, G. H. (2009b). Relationship between respiration, end-tidal CO2, and BOLD signals in resting-state fMRI. *NeuroImage* 47, 1381–1393. doi:10.1016/j.neuroimage.2009.04.048.

Chen, J. J., and Pike, G. B. (2009). BOLD-specific cerebral blood volume and blood flow changes during neuronal activation in humans. *NMR in biomedicine* 22, 1054–62. doi:10.1002/nbm.1411.

Christen, T., Jahanian, H., Ni, W. W., Qiu, D., Moseley, M. E., and Zaharchuk, G. (2015). Noncontrast mapping of arterial delay and functional connectivity using resting-state functional MRI: A study in Moyamoya patients. *Journal of Magnetic Resonance Imaging* 41, 424–430. doi:10.1002/jmri.24558.

Cohen, E. R., Ugurbil, K., and Kim, S.-G. (2002). Effect of basal conditions on the magnitude and dynamics of the blood oxygenation level-dependent fMRI response. *Journal of cerebral blood flow and metabolism : official journal of the International Society of Cerebral Blood Flow and Metabolism* 22, 1042–1053. doi:10.1097/00004647-200209000-00002.

Collins, J.-A., Rudenski, A., Gibson, J., Howard, L., and O'Driscoll, R. (2015a). Relating oxygen partial pressure, saturation and content: the haemoglobin–oxygen dissociation curve. *Breathe (Sheff)* 11, 194–201. doi:10.1183/20734735.001415.

Collins, J.-A., Rudenski, A., Gibson, J., Howard, L., and O'Driscoll, R. (2015b). Relating oxygen partial pressure, saturation and content: the haemoglobin-oxygen dissociation curve. *Breathe (Sheffield, England)* 11, 194–201. doi:10.1183/20734735.001415.

Dresel, C., Castrop, F., Haslinger, B., Wohlschlaeger, A. M., Hennenlotter, A., and Ceballos-Baumann, A. O. (2005). The functional neuroanatomy of coordinated orofacial movements: Sparse sampling fMRI of whistling. *NeuroImage* 28, 588–597. doi:10.1016/j.neuroimage.2005.06.021.

Erdoğan, S. B., Tong, Y., Hocke, L. M., Lindsey, K. P., and Blaise deB, F. (2016). Correcting for Blood Arrival Time in Global Mean Regression Enhances Functional Connectivity Analysis of Resting State fMRI-BOLD Signals. *Frontiers in human neuroscience* 10, 311.

717 doi:10.3389/fnhum.2016.00311.

718 Fagrell, B., Fronek, A., and Intaglietta, M. (1977). A microscope-television system for studying flow
719 velocity in human skin capillaries. *The American journal of physiology* 233, H318-21.

720 Fagrell, B., Intaglietta, M., and Ostergren, J. (1980). Relative hematocrit in human skin capillaries
721 and its relation to capillary blood flow velocity. *Microvascular research* 20, 327–35.
722 doi:10.1016/0026-2862(80)90033-3.

723 Fantini, S. (2014). Dynamic model for the tissue concentration and oxygen saturation of hemoglobin
724 in relation to blood volume, flow velocity, and oxygen consumption: Implications for
725 functional neuroimaging and coherent hemodynamics spectroscopy (CHS). *NeuroImage* 85,
726 202–221. doi:10.1016/j.neuroimage.2013.03.065.

727 Feinberg, D. a, Moeller, S., Smith, S. M., Auerbach, E., Ramanna, S., Gunther, M., et al. (2010).
728 Multiplexed echo planar imaging for sub-second whole brain FMRI and fast diffusion
729 imaging. *PloS one* 5, e15710. doi:10.1371/journal.pone.0015710.

730 Freire, L., and Mangin, J. F. (2001). Motion correction algorithms may create spurious brain
731 activations in the absence of subject motion. *NeuroImage* 14, 709–722.
732 doi:10.1006/nimg.2001.0869.

733 Friston, K. J., Glaser, D. E., Henson, R. N. A., Kiebel, S., Phillips, C., and Ashburner, J. (2002). Classical
734 and Bayesian inference in neuroimaging: Applications. *NeuroImage* 16, 484–512.
735 doi:10.1006/nimg.2002.1091.

736 Giller, C. A., Hatab, M. R., and Giller, A. M. (1999). Oscillations in cerebral blood flow detected with
737 a transcranial Doppler index. *Journal of cerebral blood flow and metabolism : official journal*
738 *of the International Society of Cerebral Blood Flow and Metabolism* 19, 452–9.
739 doi:10.1097/00004647-199904000-00011.

740 Glasser, M. F., Coalson, T. S., Bijsterbosch, J. D., Harrison, S. J., Harms, M. P., Anticevic, A., et al.
741 (2018). Using temporal ICA to selectively remove global noise while preserving global signal
742 in functional MRI data. *NeuroImage* 181, 692–717. doi:10.1016/j.neuroimage.2018.04.076.

743 Guyton, A. C., and Harris, J. W. (1951). Pressoreceptor-autonomic oscillation; a probable cause of
744 vasomotor waves. *The American journal of physiology* 165, 158–66.
745 doi:10.1152/ajplegacy.1951.165.1.158.

746 Herman, P., Sanganahalli, B. G., and Hyder, F. (2009). Multimodal Measurements of Blood Plasma
747 and Red Blood Cell Volumes during Functional Brain Activation. *Journal of Cerebral Blood*
748 *Flow & Metabolism* 29, 19–24. doi:10.1038/jcbfm.2008.100.

749 Hoge, R., Atkinson, J., Gill, B., Crelier, G., and Marrett, S. (1999). Investigation of BOLD signal
750 dependence on cerebral blood flow and oxygen consumption: The …. *Magnetic Resonance in*

Medicine 863, 849–863. doi:10.1002/(SICI)1522-2594(199911)42:5<849::AID-MRM4>3.0.CO;2-Z.

Hudetz, a G., Wood, J. D., Biswal, B. B., Krolo, I., and Kampine, J. P. (1999). Effect of hemodilution on RBC velocity, supply rate, and hematocrit in the cerebral capillary network. *Journal of applied physiology (Bethesda, Md. : 1985)* 87, 505–9.

Intaglietta, M. (1990). Vasomotion and flowmotion: physiological mechanisms and clinical evidence. *Vascular Medicine Review* 1, 101–112.

Intaglietta, M., Johnson, P. C., and Winslow, R. M. (1996). Microvascular and tissue oxygen distribution. *Cardiovascular research* 32, 632–43. doi:0008636396001101 [pii].

Julien, C. (2006). The enigma of Mayer waves: Facts and models. *Cardiovascular research* 70, 12–21. doi:10.1016/j.cardiores.2005.11.008.

Katura, T., Tanaka, N., Obata, A., Sato, H., and Maki, A. (2006). Quantitative evaluation of interrelations between spontaneous low-frequency oscillations in cerebral hemodynamics and systemic cardiovascular dynamics. *NeuroImage* 31, 1592–1600. doi:10.1016/j.neuroimage.2006.02.010.

Kennerley, A. J., Berwick, J., Martindale, J., Johnston, D., Papadakis, N., and Mayhew, J. E. (2005). Concurrent fMRI and Optical Measures for the Investigation of the Hemodynamic Response Function. 365, 354–365. doi:10.1002/mrm.20511.

Khalil, A. A., Villringer, K., Filleböck, V., Hu, J.-Y., Rocco, A., Fiebach, J. B., et al. (2018). Non-invasive monitoring of longitudinal changes in cerebral hemodynamics in acute ischemic stroke using BOLD signal delay. *Journal of Cerebral Blood Flow & Metabolism*, 0271678X1880395. doi:10.1177/0271678X18803951.

Killip, T. (1962). Oscillation of blood flow and vascular resistance during Mayer waves. *Circulation research* 11, 987–993. doi:10.1161/01.RES.11.6.987.

Kim, S.-G., and Ogawa, S. (2012). Biophysical and physiological origins of blood oxygenation level-dependent fMRI signals. *Journal of Cerebral Blood Flow & Metabolism* 32, 1188–1206. doi:10.1038/jcbfm.2012.23.

Kleinschmidt, A., Obrig, H., Requardt, M., Merboldt, K.-D., Dirnagl, U., Villringer, A., et al. (1996). Simultaneous Recording of Cerebral Blood Oxygenation Changes during Human Brain Activation by Magnetic Resonance Imaging and Near-Infrared Spectroscopy. *Journal of Cerebral Blood Flow & Metabolism* 16, 817–826. doi:10.1097/00004647-199609000-00006.

Krings, T., Erberich, S. G., Roessler, F., Reul, J., and Thron, A. (1999). MR blood oxygenation level-dependent signal differences in parenchymal and large draining vessels: implications for functional MR imaging. *AJNR. American journal of neuroradiology* 20, 1907–14.

785 Krings, T., Reinges, M. H. T., Erberich, S., Kemeny, S., Rohde, V., Spetzger, U., et al. (2001).
786 Functional MRI for presurgical planning: problems, artefacts, and solution strategies. *J*
787 *Neurol Neurosurg Psychiatry* 70, 749. doi:10.1136/jnnp.70.6.749.

788 Kumar, V., Croxson, P. L., and Simonyan, K. (2016). Structural Organization of the Laryngeal Motor
789 Cortical Network and Its Implication for Evolution of Speech Production. *Journal of*
790 *Neuroscience* 36, 4170–4181. doi:10.1523/JNEUROSCI.3914-15.2016.

791 Kundu, P., Inati, S. J., Evans, J. W., Luh, W.-M., and Bandettini, P. A. (2012). Differentiating BOLD and
792 non-BOLD signals in fMRI time series using multi-echo EPI. *NeuroImage* 60, 1759–70.
793 doi:10.1016/j.neuroimage.2011.12.028.

794 Liu, T. T., Nalci, A., and Falahpour, M. (2017). The global signal in fMRI: Nuisance or Information?
795 *NeuroImage* 150, 213–229. doi:10.1016/j.neuroimage.2017.02.036.

796 Lv, Y., Margulies, D. S., Cameron Craddock, R., Long, X., Winter, B., Gierhake, D., et al. (2013).
797 Identifying the perfusion deficit in acute stroke with resting-state functional magnetic
798 resonance imaging. *Annals of Neurology* 73, 136–140. doi:10.1002/ana.23763.

799 Malatino, L. S., Bellofiore, S., Costa, M. P., Lo Manto, G., Finocchiaro, F., and Di Maria, G. U. (1992).
800 Cerebral blood flow velocity after hyperventilation-induced vasoconstriction in hypertensive
801 patients. *Stroke* 23, 1728–32.

802 Mayhew, J. E. W., Askew, S., Zheng, Y., Porrill, J., Westby, G. W. M. W., Redgrave, P., et al. (1996).
803 Cerebral Vasomotion: A 0.1-Hz Oscillation in Reflected Light Imaging of Neural Activity.
804 *NeuroImage* 4, 183–93. doi:10.1006/nimg.1996.0069.

805 Mazaika, P. K., Hoeft, F., Glover, G. H., and Reiss, A. L. (2009). Methods and Software for fMRI
806 Analysis of Clinical Subjects. *NeuroImage* 47, S58. doi:10.1016/S1053-8119(09)70238-1.

807 McKay, L. C., Adams, L., Frackowiak, R. S. J., and Corfield, D. R. (2008). A bilateral cortico-bulbar
808 network associated with breath holding in humans, determined by functional magnetic
809 resonance imaging. *NeuroImage* 40, 1824–1832. doi:10.1016/j.neuroimage.2008.01.058.

810 Murphy, K., Birn, R. M., and Bandettini, P. A. (2013). Resting-state fMRI confounds and cleanup.
811 *NeuroImage* 80, 349–59. doi:10.1016/j.neuroimage.2013.04.001.

812 Murphy, K., Harris, A. D., and Wise, R. G. (2011). Robustly measuring vascular reactivity differences
813 with breath-hold: Normalising stimulus-evoked and resting state BOLD fMRI data.
814 *NeuroImage* 54, 369–379. doi:10.1016/j.neuroimage.2010.07.059.

815 Ni, L., Li, J., Li, W., Zhou, F., Wang, F., Schwarz, C. G., et al. (2017). The value of resting-state
816 functional MRI in subacute ischemic stroke: comparison with dynamic susceptibility
817 contrast-enhanced perfusion MRI. *Scientific Reports* 7, 41586. doi:10.1038/srep41586.

818 Nikulin, V. V, Fedele, T., Mehnert, J., Lipp, A., Noack, C., Steinbrink, J., et al. (2014). Monochromatic

Ultra-Slow (~0.1Hz) Oscillations in the human electroencephalogram and their relation to hemodynamics. *NeuroImage* 97, 71–80. doi:10.1016/j.neuroimage.2014.04.008.

Nishida, S., Aso, T., Takaya, S., Takahashi, Y., Kikuchi, T., Funaki, T., et al. (2018). Resting-state Functional Magnetic Resonance Imaging Identifies Cerebrovascular Reactivity Impairment in Patients With Arterial Occlusive Diseases: A Pilot Study. *Neurosurgery*. doi:10.1093/neuros/nyy434.

Obrig, H., Neufang, M., Wenzel, R., Kohl, M., Steinbrink, J., Einhäupl, K., et al. (2000). Spontaneous Low Frequency Oscillations of Cerebral Hemodynamics and Metabolism in Human Adults. *NeuroImage* 12, 623–639. doi:10.1006/nimg.2000.0657.

Ogawa, S., Menon, R. S., Kim, S. G., and Ugurbil, K. (1998). On the characteristics of functional magnetic resonance imaging of the brain. *Annu.Rev.Biophys.Biomol.Struct.* 27, 447–474. doi:10.1146/annurev.biophys.27.1.447.

Pattinson, K. T. S., Governo, R. J., MacIntosh, B. J., Russell, E. C., Corfield, D. R., Tracey, I., et al. (2009). Opioids Depress Cortical Centers Responsible for the Volitional Control of Respiration. *Journal of Neuroscience* 29, 8177–8186. doi:10.1523/JNEUROSCI.1375-09.2009.

Poline, J. B., Worsley, K. J., Evans, A. C., and Friston, K. J. (1997). Combining spatial extent and peak intensity to test for activations in functional imaging. *NeuroImage* 5, 83–96. doi:10.1006/nimg.1996.0248.

Posse, S., Wiese, S., Gembris, D., Mathiak, K., Kessler, C., Grosse-Ruyken, M. L., et al. (1999). Enhancement of BOLD-contrast sensitivity by single-shot multi-echo functional MR imaging. *Magnetic resonance in medicine* 42, 87–97.

Poulin, M. J., Liang, P. J., and Robbins, P. A. (1996). Dynamics of the cerebral blood flow response to step changes in end-tidal PCO2 and PO2 in humans. *Journal of Applied Physiology* 81, 1084–1095. doi:10.3109/11038129809035735.

Power, J. D., Barnes, K. a., Snyder, A. Z., Schlaggar, B. L., and Petersen, S. E. (2012). Spurious but systematic correlations in functional connectivity MRI networks arise from subject motion. *NeuroImage* 59, 2142–54. doi:10.1016/j.neuroimage.2011.10.018.

Power, J. D., Plitt, M., Laumann, T. O., and Martin, A. (2017). Sources and implications of whole-brain fMRI signals in humans. *NeuroImage* 146, 609–625. doi:10.1016/j.neuroimage.2016.09.038.

Radna, R. J., and MacLean, P. D. (1981). Vagal elicitation of respiratory-type and other unit responses in striopallidum of squirrel monkeys. *Brain Research* 213, 29–44. doi:10.1016/0006-8993(81)91246-4.

Rayshubskiy, A., Wojtasiewicz, T. J., Mikell, C. B., Bouchard, M. B., Timerman, D., Youngerman, B. E.,

et al. (2014). Direct, intraoperative observation of ~0.1Hz hemodynamic oscillations in awake human cortex: Implications for fMRI. *NeuroImage* 87, 323–331. doi:10.1016/j.neuroimage.2013.10.044.

Rostrup, E., Knudsen, G. M., Law, I., Holm, S., Larsson, H. B. W., and Paulson, O. B. (2005). The relationship between cerebral blood flow and volume in humans. *NeuroImage* 24, 1–11. doi:10.1016/j.neuroimage.2004.09.043.

Salimi-Khorshidi, G., Douaud, G., Beckmann, C. F., Glasser, M. F., Griffanti, L., and Smith, S. M. (2014). Automatic denoising of functional MRI data: Combining independent component analysis and hierarchical fusion of classifiers. *NeuroImage* 90, 449–468. doi:10.1016/j.neuroimage.2013.11.046.

Sassaroli, A., Pierro, M., Bergethon, P. R., and Fantini, S. (2012). Low-frequency spontaneous oscillations of cerebral hemodynamics investigated with near-infrared spectroscopy: A review. *IEEE Journal on Selected Topics in Quantum Electronics* 18, 1478–1492. doi:10.1109/JSTQE.2012.2183581.

Satow, T., Aso, T., Nishida, S., Komuro, T., Ueno, T., Oishi, N., et al. (2017). Alteration of Venous Drainage Route in Idiopathic Normal Pressure Hydrocephalus and Normal Aging. *Frontiers in Aging Neuroscience* 9. doi:10.3389/fnagi.2017.00387.

Satterthwaite, T. D., Elliott, M. A., Gerraty, R. T., Ruparel, K., Loughead, J., Calkins, M. E., et al. (2013). An improved framework for confound regression and filtering for control of motion artifact in the preprocessing of resting-state functional connectivity data. *NeuroImage* 64, 240–256. doi:10.1016/J.NEUROIMAGE.2012.08.052.

Siegel, A. M., Culver, J. P., Mandeville, J. B., and Boas, D. A. (2003). Temporal comparison of functional brain imaging with diffuse optical tomography and fMRI during rat forepaw stimulation. *Physics in medicine and biology* 48, 1391–403.

Simonyan, K., and Jürgens, U. (2003). Efferent subcortical projections of the laryngeal motorcortex in the rhesus monkey. *Brain Research* 974, 43–59. doi:10.1016/S0006-8993(03)02548-4.

Smith, S. M., Beckmann, C. F., Andersson, J., Auerbach, E. J., Bijsterbosch, J., Douaud, G., et al. (2013). Resting-state fMRI in the Human Connectome Project. *NeuroImage* 80, 144–168. doi:10.1016/j.neuroimage.2013.05.039.

Smith, S. M., Jenkinson, M., Woolrich, M. W., Beckmann, C. F., Behrens, T. E. J., Johansen-Berg, H., et al. (2004). Advances in functional and structural MR image analysis and implementation as FSL. *NeuroImage* 23 Suppl 1, S208-19. doi:10.1016/j.neuroimage.2004.07.051.

Taylor Webb, J., Ferguson, M. a., Nielsen, J. a., and Anderson, J. S. (2013). BOLD granger causality reflects vascular anatomy. *PLoS ONE* 8, 1–19. doi:10.1371/journal.pone.0084279.

887 Tgavalekos, K. T., Kainerstorfer, J. M., Sassaroli, A., and Fantini, S. (2016). Blood-pressure-induced
888 oscillations of deoxy- and oxyhemoglobin concentrations are in-phase in the healthy breast
889 and out-of-phase in the healthy brain. *Journal of Biomedical Optics* 21, 101410.
890 doi:10.1117/1.JBO.21.10.101410.

891 Thomas, D. L., Lythgoe, M. F., Pell, G. S., Calamante, F., and Ordidge, R. J. (2000). The measurement
892 of diffusion and perfusion in biological systems using magnetic resonance imaging. *Physics in*
893 *medicine and biology* 45, R97-138. doi:10.1088/0031-9155/45/8/201.

894 Tian, F., Niu, H., Khan, B., Alexandrakis, G., Behbehani, K., and Liu, H. (2011). Enhanced Functional
895 Brain Imaging by Using Adaptive Filtering and a Depth Compensation Algorithm in Diffuse
896 Optical Tomography. *IEEE Transactions on Medical Imaging* 30, 1239–1251.
897 doi:10.1109/TMI.2011.2111459.

898 Tong, Y., and Frederick, B. deB (2014). Tracking cerebral blood flow in BOLD fMRI using recursively
899 generated regressors. *Human brain mapping* 35, 5471–85. doi:10.1002/hbm.22564.

900 Tong, Y., Hocke, L. M., Licata, S. C., and Frederick, B. deB (2012). Low-frequency oscillations
901 measured in the periphery with near-infrared spectroscopy are strongly correlated with
902 blood oxygen level-dependent functional magnetic resonance imaging signals. *Journal of*
903 *biomedical optics* 17, 106004. doi:10.1117/1.JBO.17.10.106004.

904 Tong, Y., Lindsey, K. P., Hocke, L. M., Vitaliano, G., Mintzopoulos, D., and Frederick, B. deB (2017).
905 Perfusion information extracted from resting state functional magnetic resonance imaging.
906 *Journal of cerebral blood flow and metabolism : official journal of the International Society of*
907 *Cerebral Blood Flow and Metabolism* 37, 564–576. doi:10.1177/0271678X16631755.

908 Tong, Y., Yao, J. F., Chen, J. J., and Frederick, B. deB (2018). The resting-state fMRI arterial signal
909 predicts differential blood transit time through the brain. *Journal of cerebral blood flow and*
910 *metabolism : official journal of the International Society of Cerebral Blood Flow and*
911 *Metabolism*, 271678X17753329. doi:10.1177/0271678X17753329.

912 Tuunanen, P. I., and Kauppinen, R. A. (2006). Effects of oxygen saturation on BOLD and arterial spin
913 labelling perfusion fMRI signals studied in a motor activation task. *NeuroImage* 30, 102–9.
914 doi:10.1016/j.neuroimage.2005.09.021.

915 Uludağ, K., and Blinder, P. (2018). Linking brain vascular physiology to hemodynamic response in
916 ultra-high field MRI. *NeuroImage* 168, 279–295. doi:10.1016/j.neuroimage.2017.02.063.

917 Van Dijk, K. R. A., Sabuncu, M. R., and Buckner, R. L. (2012). The influence of head motion on
918 intrinsic functional connectivity MRI. *NeuroImage* 59, 431–8.
919 doi:10.1016/j.neuroimage.2011.07.044.

920 Winder, A. T., Echagarruga, C., Zhang, Q., and Drew, P. J. (2017). Weak correlations between
921 hemodynamic signals and ongoing neural activity during the resting state. *Nature*

neuroscience 20, 1761–1769. doi:10.1038/s41593-017-0007-y.

Wise, R. G., Ide, K., Poulin, M. J., and Tracey, I. (2004). Resting fluctuations in arterial carbon dioxide induce significant low frequency variations in BOLD signal. *NeuroImage* 21, 1652–64. doi:10.1016/j.neuroimage.2003.11.025.

Wu, C. W., Gu, H., Zou, Q., Lu, H., Stein, E. A., and Yang, Y. (2012). TE-dependent spatial and spectral specificity of functional connectivity. *NeuroImage* 59, 3075–84. doi:10.1016/j.neuroimage.2011.11.030.

Yablonskiy, D. A., and Haacke, E. M. (1994). Theory of NMR signal behavior in magnetically inhomogeneous tissues: the static dephasing regime. *Magnetic resonance in medicine* 32, 749–63.

Yen, C. C.-C., Papoti, D., and Silva, A. C. (2017). Investigating the spatiotemporal characteristics of the deoxyhemoglobin-related and deoxyhemoglobin-unrelated functional hemodynamic response across cortical layers in awake marmosets. *NeuroImage* 7, 83–8. doi:10.1016/j.neuroimage.2017.03.005.

Zhu, D. C., Tarumi, T., Khan, M. A., and Zhang, R. (2015). Vascular coupling in resting-state fMRI: evidence from multiple modalities. *Journal of cerebral blood flow and metabolism : official journal of the International Society of Cerebral Blood Flow and Metabolism* 35, 1910–20. doi:10.1038/jcbfm.2015.166.